

Submitted to ApJ

The Massive Triple Star System HD 16429 A

M. V. McSwain¹

*Center for High Angular Resolution Astronomy
 Department of Physics and Astronomy, P.O. Box 4106
 Georgia State University, Atlanta, GA 30302-4106
 Electronic mail: mcswain@chara.gsu.edu*

ABSTRACT

HD 16429 A is a triple star system consisting of a single-lined spectroscopic binary and a widely separated third component, previously identified via speckle interferometry. Here I present the first orbital elements for the unblended spectroscopic binary as well as estimates of the spectral types and relative flux contributions for each visible component based upon a Doppler tomographic reconstruction of their spectra. There are several stars around HD 16429 A, including the nearby Be X-ray binary and microquasar LS I +61°303, which all probably belong to a sub-cluster within the Cas OB6 association.

Subject headings: binaries: spectroscopic — stars: early-type — stars: individual (HD 16429, HIP 12495, V482 Cas, SAO 12383, BD+60°541, V615 Cas, LS I +61°303)

1. Introduction

O-type stars are most commonly found within young open clusters and OB associations in the spiral arms of the Galaxy (Gies 1987), and the binary frequency among these cluster and association members is significantly higher (between 70 – 75%) than among field O stars (19 – 22%) and runaways (about 8%) (Gies 1987; Garmann 1994; Mason et al. 1998).

¹Visiting Astronomer, Kitt Peak National Observatory, National Optical Astronomy Observatories, operated by the Association of Universities for Research in Astronomy, Inc., under contract with the National Science Foundation.

Multiple O star systems in clusters are particularly influential in the dynamics of the cluster because stars will be ejected both through supernova explosions in close binaries and through close gravitational encounters of stars with binaries. Triple O star systems containing a close pair and a more widely separated component are particularly important sites of gravitational interactions (Mason et al. 1998).

HD 16429 A (HIP 12495, V482 Cas, SAO 12383, BD+60°541) is an O9.5 II ((n)) star (Walborn 1976) and a member of the Cas OB6 association (Garmany & Stencel 1992). It has two optical companions, component B at a separation of 6.66 arcsec, and C at a separation of 53.2 arcsec (Mason et al. 1998). HD 16429 B is an F4 V star (Meisel 1968), which indicates that it is not physically associated with A. Component C is more likely associated based upon its magnitude and color (see §4). The A component was itself found to be a speckle binary with a separation of 0.30 arcsec (Mason et al. 1998). Gies & Bolton (1986) found that one component of A may also be a spectroscopic binary, making it a triple system, but they were unable to identify the period of this close pair. All of the components of the hierarchical HD 16429 system are shown in Figure 1. Other observations have shown HD 16429 A to be a radio emitter (Martí et al. 1998) as well as a weak X-ray source (Goldoni & Mereghetti 1995). The radio and X-ray emission probably originates in the stellar winds (Martí et al. 1998).

Here I present evidence to confirm that HD 16429 A is a triple star system with a spectroscopic binary component (HD 16429 Ab1) and a radial velocity stationary companion (HD 16429 Aa). The Aa and Ab1 components were isolated using a Doppler tomography algorithm, but the Ab2 component remains hidden. Approximate spectral types and relative flux contributions are presented for the two visible components. Finally, I discuss the stars in the immediate vicinity of HD 16429 A and their relationship to the Cas OB6 association.

2. Observations and Blended Line Radial Velocities

Thirty-five optical spectra of HD 16429 A were obtained with the Kitt Peak National Observatory 0.9-m Coudé Feed Telescope during runs in 2000 October and 2000 December. The spectra have a resolving power $R = \lambda/\delta\lambda = 9500$ using the long collimator, grating B (in second order with order sorting filter OG550), camera 5, and the F3KB CCD, a Ford Aerospace 3072 \times 1024 device. These arrangements produced a spectral coverage of 6440–7105 Å. Usually two exposures of 15 minutes duration were taken each night, separated by 2–3 hours. The spectrum of the rapidly rotating A-type star, ζ Aql, was observed each night for removal of atmospheric water vapor and O₂ bands. Also, the O-type stars HD 34078 and HD 47839 were observed as spectral comparisons. Each set of observations was

accompanied by numerous bias, flat field, and Th Ar comparison lamp calibration frames. The dates of observation are given in Table 1.

The spectra were extracted and calibrated using standard routines in IRAF². All the spectra were rectified to a unit continuum by fitting line-free regions. The removal of atmospheric lines was done by creating a library of ζ Aql spectra from each run, removing the broad stellar features from these, and then dividing each target spectrum by the modified atmospheric spectrum that most closely matched the target spectrum in a selected region dominated by atmospheric absorptions. Some glitches appeared as artifacts of the removal of the atmospheric telluric lines, and these were excised by linear interpolation. The spectra from each run were then transformed to a common heliocentric wavelength grid.

Radial velocities were measured by fitting a parabola to the line cores of H α , He I $\lambda 6678$, and He I $\lambda 7065$, but several factors made it difficult to obtain consistent measurements. The H α line shows variable P Cygni emission that pushes the line’s center blueward. Due to this certain contamination, radial velocities from the H α line were not used. In addition, measurements of the He I $\lambda 7065$ line have a slightly lower mean radial velocity than the mean for the He I $\lambda 6678$ line. This could be due to different relative line strengths of the He I lines in the blended stars, contamination from He II $\lambda 6683$ absorption in one component, or a radial velocity gradient due to outflowing winds (see §4). However, the difference in their mean velocities is small and only corresponds to a difference of 1.4 pixels on the chip, so the mean velocity of the two He I lines was used in this analysis.

To account for small deviations in radial velocity due to the wavelength calibration, the interstellar lines present in the spectra were inspected. A large number of interstellar features were identified from the lists of Herbig (1975), Herbig & Leka (1991), Morton (1991), and especially Galazutdinov et al. (2000). An interstellar spectrum was created by extracting these lines from the mean HD 16429 spectrum, and then it was cross correlated with each individual spectrum to measure any systematic radial velocity shift (generally $< 7 \text{ km s}^{-1}$). The velocity shift was subtracted from the measured radial velocities, and the resulting velocities are shown in the third column of Table 1. In the next section, I will show that these radial velocities actually represent the results of line blending between a single-lined spectroscopic binary and a stationary component.

²IRAF is distributed by the National Optical Astronomy Observatories, which is operated by the Association of Universities for Research in Astronomy, Inc., under cooperative agreement with the National Science Foundation.

3. Orbital Elements from a Two Component Model

Visual inspection of the spectra revealed radial velocity variations indicative of an orbital period of about 3 days, but a more precise period search was done using a version of the discrete Fourier transform and CLEAN deconvolution algorithm of Roberts, Lehár, & Dreher (1987) (written in IDL³ by A. W. Fullerton). The most significant signal found in the CLEANed power spectrum occurs at the period $P = 3.051$ d. Relics of this signal also occur at integer multiples of this frequency, but the true period cannot be shorter because there are no significant changes in radial velocity over the 2 – 3 hour intervals between the observations from a given night.

This period was used with the non-linear, least-squares fitting program of Morbey & Brosterhus (1974) to solve for the orbital elements. The best fit was obtained by allowing the period to vary slightly, to an improved value of $P = 3.0539$ d, and assigning only half weight to one point with very large scatter near 0.95 phase. The resulting preliminary orbital elements are listed in the second column of Table 2, and the radial velocity curve is illustrated in Figure 2 with the dotted line. Note that this curve has been shifted in phase so that the epoch, T , corresponds to the final time of periastron, discussed below. The observed minus calculated velocity errors ($O - C$) based on this preliminary solution are given in Table 1, column 4. The root-mean-square of the velocity residuals is comparable to the scatter in the best measured lines.

There are a number of other radial velocity measurements for HD 16429 A in the literature (10 by Abt, Levy, & Gendet (1972), 15 by Gies & Bolton (1986), and 1 by Conti, Leep, & Lorre (1977)), so these measurements were combined with those in Table 1 to refine the orbital period. Since each investigation used different spectral lines and wavelength regions to measure velocities, the results may have systematic differences. However, the agreement between data sets was reasonable, and including the additional measurements significantly improved the orbital period, $P = 3.05442 \pm 0.00005$ d.

The speckle results (Mason et al. 1998) indicate that at least two bright components were recorded in these spectra, so I created grayscale images of the spectral lines as a function of orbital phase to search for evidence of multiple components. Figure 3 shows the plot of the He I $\lambda 6678$ line. It clearly reveals signs of a single-lined spectroscopic binary, Ab1, superimposed upon a stationary component, Aa, with similar systemic velocity, consistent with expectations from the speckle observations. Because the stationary component's lines are blended with the moving component, the preliminary radial velocity semiamplitude of

³IDL is a registered trademark of Research Systems, Inc.

the moving component is probably greatly underestimated, and perhaps the preliminary eccentricity and longitude of periastron are misrepresented as well.

To determine the true orbital elements of the Ab1 component, the Aa component was isolated using a two-component tomographic separation and then subtracted from the observations. Tomographic separation relies upon the radial velocity estimates of the stars and their flux ratio to recreate the spectra of the individual stars (Bagnuolo & Gies 1991). The algorithm uses the observed composite spectra, approximate flux ratios of the stars, the center of mass velocity, V_0 , and the velocity semi-amplitude, K , of component Ab1 to calculate the solution using an iterative least squares technique. For the Aa component, the velocity amplitude was set to 0. A three-component separation was not attempted because of the extreme faintness of the Ab2 spectroscopic component. Even the two-component separation was difficult because the true velocity amplitude, K , of Ab1 is unknown, and visual inspection of Figure 2 reveals that it could be as high as 200 km s^{-1} . The tomographic separation is not very sensitive to the choice of the relative flux contribution of the components. Initially, an equal flux contribution was assumed, and the value was later refined according to the methods discussed in the following section.

I computed tomographic separations for a grid of assumed semi-amplitudes for $30 < K < 200 \text{ km s}^{-1}$. In order to identify the best fit value of K , I used the separated components to recreate a set of synthetic spectra for each observation which was then compared to the original spectra. The He I $\lambda 6678$ and He I $\lambda 7065$ line regions were used separately to compute the χ^2 error between the observed and recreated spectra. The errors associated with the He I $\lambda 7065$ line were slightly larger because that line is located in a region with many atmospheric telluric lines, so it was correspondingly noisier after the telluric removal process. The values of K corresponding to the minimum error for each line were then averaged to obtain the optimal value of $K = 124 \pm 25 \text{ km s}^{-1}$.

Once the Aa component was isolated, I subtracted its profile from the observed spectra to attain profiles of the Ab1 component alone, and then I measured the radial velocities of Ab1 in the same way as before. These unblended radial velocities are listed in column 5 of Table 1. The new orbital elements of the spectroscopic binary were calculated using the same technique discussed above and are included in the last column of Table 2. Table 1, column 2 lists the orbital phase from periastron based on this final solution. Although the optimal K is $124 \pm 25 \text{ km s}^{-1}$, the orbital fitting program found a slightly higher value of $K = 136 \pm 6 \text{ km s}^{-1}$, but these estimates are consistent within errors. Figure 2 includes the final radial velocities for the moving component as the solid points and the theoretical radial velocity curve as the solid line, and the new grayscale plot of the isolated moving component is shown in Figure 4. The signal to noise ratio is too low to positively identify

the anti-phase motion of the spectroscopic companion Ab2 in this plot.

4. Discussion

The flux ratio of the two visible components of HD 16429 A was determined using their observed speckle magnitudes, $\delta m_V = 0.5 \pm 0.2$ (Mason & Hartkopf 2001, private communication). The stationary star contributes a stronger signal in the spectra, and it is also the brighter component with 61 ± 5 % of the overall luminosity. This star is HD 16429 Aa described by Mason et al. (1998), whereas the visible moving component is HD 16429 Ab1. The flux ratio can also be estimated using the equivalent width of each component's He I $\lambda 6678$ line. Conti (1974) found that in late O stars of all luminosity classes, the equivalent width of this line is roughly constant (but with a large scatter), and I adopted the method of Petrie (1939) to determine the flux ratio of the stars from their observed equivalent widths. Assuming an intensity ratio $r = F_2/F_1$ for the tomographic reconstruction, the resulting equivalent widths of the reconstructed moving and stationary component spectra are A_1 and A_2 , respectively. The relative continuum intensities are then $1/(1+r)$ and $r/(1+r)$, respectively, and the absolute line strengths are $s_1 = A_1/(1+r)$ and $s_2 = rA_2/(1+r)$. Because the true strengths of the lines are the same in each star, the true intensity ratio is $r_1 = rA_2/A_1$. By integrating over the He I $\lambda 6678$ line in each component and comparing their equivalent widths, the contribution of the stationary component was found to be about 70 ± 7 % of the system's total luminosity. This value agrees reasonably well with that obtained from speckle observations, but is less accurate because of the intrinsic scatter in the He I $\lambda 6678$ widths, so I adopted the flux ratio from the speckle observations.

Figure 5 presents a plot of the reconstructed spectra, using the final $K = 136 \text{ km s}^{-1}$ and normalized for their flux contribution. The figure also shows the Aa and Ab1 components compared to two stars of similar spectral type, HD 34078 and HD 47839. The comparison spectra have been smoothed using a Gaussian profile so that their FWHM and line depths more closely match those of the separated components. This smoothing does not significantly affect the equivalent widths of the lines. The spectra of the Aa and Ab1 components have also been smoothed slightly to reduce noise.

The tomographic separation of the spectra revealed that both visible components of HD 16429 A have strong H α and He I lines. The smoothed spectra of HD 34078 and HD 47839 have He I lines of similar strength, although stronger H α profiles. H α emission is common in luminous O stars (luminosity classes I, II, and III), so the difference in line strengths is likely due to emission in HD 16429 A. (HD 34078 and HD 47839 are both main sequence O stars with no emission.) The emission may not have been distributed properly

between the two component stars during the tomographic separation because it varies on a non-orbital timescale. The original blended spectra showed striking P Cygni emission in the H α line, which is associated almost entirely with the Aa component in the reconstructions. This widely-separated member of the triple system is probably the more evolved of the group since it has such strong emission from stellar winds. Since it is the more luminous, the stationary component corresponds to the O9.5 II type that was assigned to the system by Walborn (1976). The ((n)) suffix used by Walborn to indicate slightly broadened lines probably reflects the line blending with the Ab1 component. The He I line strengths are similar to those in HD 34078, an O9.5 V star. The absence of significant He II provides further confirmation of the spectral type.

The separation also revealed weak He II $\lambda\lambda 6527, 6683$, and 6891 absorption in the Ab1 component. He II lines only appear in O spectra, disappearing entirely in the earliest B spectra. Their presence indicates that this star is hotter than the brighter Aa star. Comparing the strengths of these lines with those in HD 47839 reveals that the moving component is a slightly later, O8 spectral type, although the luminosity class cannot be specified by the comparison. However, the difference in speckle magnitudes is consistent with an O8 III-V classification for HD 16429 Ab1 (Howarth & Prinja 1989).

The second spectroscopic companion, Ab2, remains hidden even after the tomographic separation (Fig. 4), but the statistical method of Mazeh & Goldberg (1992) suggests that it is a massive, early B-type star. For single-lined spectroscopic binaries consisting of a primary of mass M_1 and a secondary of mass M_2 , with a mass ratio $q = M_2/M_1$, the mass function is given by $f(M_2) = M_1 \sin^3 i q^3/(1 + q)^2$. It cannot be solved uniquely for both q and i , but Mazeh & Goldberg recommend an iterative solution based on a random distribution of both parameters. Given the known mass function and the primary mass, the mass ratio can be calculated for each possible inclination and then averaged over the range of inclinations. Using a mass of $28 - 33M_\odot$ for the O8 III-V primary (Howarth & Prinja 1989) and $f(M_2) = 0.76 \pm 0.11$ from the final orbital solution, the probable mass ratio is 0.6. This is inconsistent with a low mass compact companion, but suggests instead a $17 - 20M_\odot$ early B-type star (Howarth & Prinja 1989). The Ab2 component remains hidden because its flux is overwhelmed by the two brighter O stars. If these masses are adopted, then the orbital inclination is approximately $i = 42^\circ$, and no eclipses are expected (or observed by Hipparcos; Perryman et al. 1997).

There are several stars in the vicinity of HD 16429 A, including the Be X-ray binary LS I +61°303, that have similar radial velocities, proper motions, apparent V magnitudes, and $B - V$ colors (summarized in Table 3). Parabolic fits of the He I $\lambda 6678$ and He I $\lambda 7065$ lines in the tomographically isolated spectrum of the Aa component provided its average

radial velocity of -26 ± 5 km s $^{-1}$. This is somewhat different than the systemic velocity of the spectroscopic pair, -49.5 ± 3.3 km s $^{-1}$. However, the observed difference in V_0 in HD 16429 Aa and Ab1 is probably due to differing wind velocities of the two stars. Radial velocities of photospheric lines are known to reflect the outward acceleration of the line formation region (Conti, Garmany, & Hutchings 1977; Bohannan & Garmany 1978). LS I +61°303 has a systemic velocity $V_0 = -55 \pm 6$ km s $^{-1}$ (Hutchings & Crampton 1981). No radial velocities are available for HD 16429 C or ALS 7378. The proper motion of each star is from the Simbad database. For HD 16429 Aa and Ab1, V and $B - V$ were found using the values from Hiltner (1956) and the flux ratio determined above. For LS I +61°303, those values were found by averaging those by Drilling (1975) and Coyne & MacConnell (1983). LS I +61°303 has a somewhat redder $B - V$ than the other stars, but it has previously been identified with the Cas OB6 association by Steele et al. (1998). V and $B - V$ for the remaining stars are from the Simbad database. Based on these similarities, HD 16429 A and its neighbors probably make up a small sub-cluster within the Cas OB6 association.

The stars in this sub-cluster were probably born in the same generation of star formation and therefore have approximately the same age and distance. Garmany & Stencel (1992) used main sequence fitting to determine a distance of 2.40 ± 0.18 kpc to the Cas OB6 association. However, Frail & Hjellming (1991) used a kinematical model of the Galaxy to determine the distance to LS I +61°303 based on the velocities of H I absorption lines in its spectrum, and they placed that system at a closer distance of 2.0 ± 0.2 kpc (confirmed by Steele et al. (1998)). Therefore I adopted a distance of 2.0 kpc for the group. Placing the stars on evolutionary tracks in a color-magnitude diagram is difficult since the reddening is variable across the association (Hanson & Clayton 1993). For HD 16429 A, the spectral type of each component was used to obtain its intrinsic $B - V$ (Wegner 1994), which was then combined with the observed $B - V$ for the system (Hiltner 1956) to determine its reddening, $E(B - V)$, and absolute magnitude, M_V . Howarth (1983) provides $E(B - V) = 0.75$ for LS I +61°303. The reddening of HD 16429 C and ALS 7378 was estimated assuming that each is a B0 V star (based on their B and V magnitudes relative to HD 16429 A) and following the same procedure used for HD 16429 A. Table 3 also lists the $E(B - V)$ and M_V for each star in the sub-cluster.

Böhm-Vitense (1981) provides temperatures of massive stars based on their spectral types, and I used her calibration to find their temperatures and bolometric corrections (Howarth & Prinja 1989). Their luminosities were found using the expression $\log L/L_\odot = -0.4(M_{bol} - 4.74)$. The evolutionary tracks for non-rotating stars of Schaller et al. (1992), based on $\log T$ and $\log L/L_\odot$, provide estimates of the current and initial stellar masses as well as stellar ages, and these are also included in Table 3. It is interesting to note that

the initial mass of HD 16429 Aa places a lower limit on the initial mass of the neutron star progenitor in LS I +61°303. It must have originated in a star with more than $39 M_{\odot}$ when the group formed 2 – 4 Myr ago to have evolved more quickly than HD 16429 Aa.

I especially thank Douglas Gies for his advice and comments regarding this manuscript. I also thank David Wingert and Wenjin Huang for taking many of the observations, and the KPNO staff for their assistance and travel support. I am also grateful to Dr. Alex Fullerton for sharing his period search code, and to Brian Mason and William Hartkopf of the U.S. Naval Observatory for sending me information from their speckle interferometric observations. This research has made use of the SIMBAD database, operated at CDS, Strasbourg, France. Financial support was provided by the National Science Foundation through grant AST–0205297 (DRG). Institutional support has been provided from the GSU College of Arts and Sciences and from the Research Program Enhancement fund of the Board of Regents of the University System of Georgia, administered through the GSU Office of the Vice President for Research. I gratefully acknowledge all this support.

REFERENCES

Abt, H. A., Levy, S. G., & Gendet, T. L. 1972, AJ, 77, 138

Bagnuolo, W. G. Jr., & Gies, D. R. 1991, ApJ, 376, 266

Bohannan, B., & Garmany, C. D. 1978, ApJ, 223, 908

Böhm-Vitense, E. 1981, ARA&A, 19, 295

Conti, P. S. 1974, ApJ, 187, 539

Conti, P. S., Garmany, C. D., & Hutchings, J. B. 1977, ApJ, 215, 561

Conti, P. S., Leep, E. M., & Lorre, J. J. 1977, ApJ, 214, 759

Coyne, G. V., & MacConnell, D. J. 1983, Vatican Obs. Pub., 2, 73

Drilling, J. S. 1975, AJ, 80, 128

Frail, D. A., & Hjellming, R. M. 1991, AJ, 101, 2126

Galazutdinov, G. A., Musaev, F. A., Krelowski, J., & Walker, G. A. H. 2000, PASP, 112, 648

Garmany, C. D. 1994, PASP, 106, 25

Garmany, C. D., & Stencel, R. E. 1992, A&AS, 94, 211

Gies, D. R. 1987, ApJS, 64, 545

Gies, D. R., & Bolton, C. T. 1986, ApJ, 61, 419

Goldoni, P., & Mereghetti, S. 1995, A&A, 299, 751

Hanson, M. M., & Clayton, G. C. 1993, AJ, 106, 1947

Herbig, G. H. 1975, ApJ, 196, 129

Herbig, G. H., & Leka, K. D. 1991, ApJ, 382, 193

Hiltner, W. A. 1956, ApJS, 2, 389

Howarth, I. D. 1983, MNRAS, 203, 801

Howarth, I. D., & Prinja, R. K. 1989, ApJS, 69, 527

Hutchings, J. B., & Crampton, D. 1981, PASP, 93, 486

Martí, J., Peracaula, M., Paredes, J. M., Massi, M., & Estalella, R. 1998, A&A, 329, 951

Mason, B. D., Gies, D. R., Hartkopf, W. I., Bagnuolo, W. G., ten Brummelaar, T., McAlister, H. A. 1998, AJ, 115, 821

Mazeh, T., & Goldberg, D. 1992, ApJ, 394, 592

Meisel, D. D. 1968, AJ, 73, 350

Morbey, C. L., & Brosterhus, E. B. 1974, PASP, 86, 455

Morton, D. C. 1991, ApJS, 77, 119

Perryman, M. A. C., et al. 1997, A&A, 323, L49

Petrie, R. M. 1939, Publ. Dom. Ap. Obs. Victoria, 7, 205

Roberts, D. H., Lehár, J., & Dreher, J. W. 1987, AJ, 93, 968

Schaller, G., Schaefer, D., Meynet, G., & Maeder, A. 1992, A&AS, 96, 269

Steele, I. A., Negueruela, I., Coe, M. J., & Roche, P. 1998, MNRAS, 297, L5

Walborn, N. R. 1976, ApJ, 205, 419

Wegner, W. 1994, MNRAS, 270, 229

Table 1. Journal of Spectroscopy

Date (HJD-2,450,000)	Orbital Phase	V_r (blend) (km s $^{-1}$)	$O - C$ (km s $^{-1}$)	V_r (final) (km s $^{-1}$)	$O - C$ (km s $^{-1}$)
1817.877	0.334	-21.4	3.3	-12.5	-15.9
1818.881	0.663	-4.6	14.9	16.7	-25.7
1819.766	0.953	-42.0	30.0	-193.8	-11.7
1820.879	0.317	-23.9	3.2	-35.4	-28.5
1821.833	0.629	12.0	29.1	44.6	-8.4
1822.857	0.964	-64.7	9.9	-201.9	-12.3
1823.806	0.275	-31.6	2.3	-30.8	4.4
1823.915	0.311	-27.7	0.2	-26.7	-16.1
1824.817	0.606	-9.4	6.5	38.1	-19.9
1824.942	0.647	-0.6	17.7	43.6	-4.2
1830.834	0.576	-1.8	13.0	31.6	-30.6
1830.938	0.610	1.0	17.1	39.7	-17.6
1888.817	0.559	-0.7	13.5	82.6	19.2
1889.816	0.886	-56.9	-1.1	-118.6	6.1
1890.721	0.183	-46.8	8.3	-122.1	-11.0
1890.801	0.209	-48.2	0.1	-108.0	-19.8
1892.715	0.835	-59.0	-14.9	-94.6	-19.9
1892.867	0.885	-62.1	-6.5	-126.4	-2.7
1893.740	0.171	-56.6	1.5	-110.8	10.4
1893.884	0.218	-45.5	0.4	-67.0	13.3
1894.760	0.505	6.5	20.4	87.7	26.0
1895.715	0.818	-41.7	-1.2	-51.5	6.7
1895.804	0.847	-47.2	-0.6	-63.3	22.5
1896.645	0.122	-69.0	2.2	-154.3	8.0
1896.778	0.166	-61.9	-2.3	-121.8	3.9
1897.646	0.450	-2.4	12.9	69.5	17.9
1897.778	0.493	-10.9	3.1	70.3	10.1
1898.650	0.779	-37.7	-4.1	-34.7	-9.8
1898.782	0.822	-47.8	-6.4	-63.6	-1.5
1899.652	0.107	-57.1	17.8	-161.2	12.6

Table 1—Continued

Date (HJD-2,450,000)	Orbital Phase	V_r (blend) (km s $^{-1}$)	$O - C$ (km s $^{-1}$)	V_r (final) (km s $^{-1}$)	$O - C$ (km s $^{-1}$)
1899.784	0.150	−58.9	5.0	−136.9	2.5
1900.647	0.433	−11.5	4.6	70.7	24.0
1900.778	0.476	−0.6	13.8	80.4	23.0
1901.631	0.755	−25.1	4.7	18.2	25.1
1901.764	0.798	−36.8	0.1	−20.7	20.2

Table 2. Orbital Elements

Element	Blend	Final Value
P (d)	3.054 (5)	3.05442 ^a
T (HJD – 2,450,000)	1892.44 (29)	1893.22 (10)
K (km s ⁻¹)	35.1 (18)	136 (6)
V_0 (km s ⁻¹)	–33.5 (11)	–50 (3)
e	0.08 (6)	0.17 (4)
ω (°)	80 (30)	169 (12)
r.m.s. (km s ⁻¹)	6.5	18.0
$f(m)$ (M_\odot)	0.014 (2)	0.76 (11)
$a_1 \sin i$ (R_\odot)	2.1 (1)	8.1 (4)

Note. — The parenthetic numbers are the standard errors in the last digit quoted (decimals omitted).

^aFixed.

Table 3. Associated Stars Near HD 16429

Element	HD 16429 Aa	HD 16429 Ab1	HD 16429 C	ALS 7378	LS I +61° 303
Separation (arcmin)	0.9	1.4	3.6
Radial Velocity (km s ⁻¹)	-26 (5)	-50 (3)	...	-55 (6)	...
μ_α (mas yr ⁻¹)	-5.8 (21)	...	-4 (4)	4 (4)	0.6 (22)
μ_δ (mas yr ⁻¹)	3.1 (12)	...	6.3 (16)	-1.7 (26)	1.6 (14)
<i>V</i>	8.2	8.7	10.8	11.0	10.76
<i>B</i> - <i>V</i>	0.64	0.59	0.46	0.4	0.83
<i>E</i> (<i>B</i> - <i>V</i>)	0.88 (3)	0.88 (2)	0.72 (2)	0.66 (2)	0.75 (2)
<i>M_V</i> (<i>d</i> = 2.0 kpc)	-6.0 (5)	-5.5 (5)	-2.9 (5)	-2.6 (5)	-3.1 (5)
log <i>T</i> (K)	4.51 (2)	4.55 (1)	4.47 (1)	4.47 (1)	4.47 (1)
log <i>L</i> / <i>L</i> _⊙	5.57 (26)	5.44 (23)	4.20 (23)	4.08 (23)	4.28 (23)
Initial <i>M</i> (<i>M</i> _⊙)	39 (13)	36 (9)	13.6 (17)	13.0 (16)	14.1 (18)
Current <i>M</i> (<i>M</i> _⊙)	37 (11)	35 (8)	13.6 (17)	13.0 (16)	14.1 (18)
Age (Myr)	3.8 (9)	3.4 (5)	1.2 (2.8)	2.1 (10)	3.0 (18)

15

Note. — The errors are presented in the same format as Table 2. Errors in *E*(*B* - *V*) and *M_V* are based on errors in the intrinsic (*B* - *V*) color and distance. The error in log *T* is based on the temperature difference between adjacent spectral types (Böhm-Vitense 1981), and the remaining errors follow from these.

Fig. 1.— The various components of the HD 16429 system are shown. The B component is a chance optical alignment and is not physically associated with the group. Its V magnitude is from the Washington Double Star Catalog (<http://ad.usno.navy.mil/wds/>), and all other spectral types and magnitudes are discussed in the text.

Fig. 2.— The radial velocity measurements of the blended components (*open circles*) and the preliminary orbital solution (*dotted line*) are plotted against the final orbital phase. Also plotted are the radial velocity measurements of the isolated spectroscopic component (*filled circles*) and its orbital solution (*solid line*). Phase zero corresponds to periastron.

Fig. 3.— The He I $\lambda 6678$ line is shown in linear plots (above) and as a grayscale image (below) which shows a blend of the moving and stationary components. The intensity at each velocity in the grayscale image is assigned one of 16 gray levels based on its value between the minimum (dark) and maximum (bright) observed values. The intensity between observed spectra is calculated by a linear interpolation between the closest observed phases (shown by arrows along the right axis). The solid white line shows the theoretical velocity curve of the blended solution.

Fig. 4.— The He I $\lambda 6678$ line for the isolated moving component is shown in the same format as Fig. 3.

Fig. 5.— The separated Aa and Ab1 components of HD 16429 are shown with the spectral comparison stars HD 34078 and HD 47839. Their rectified fluxes are offset vertically for clarity.

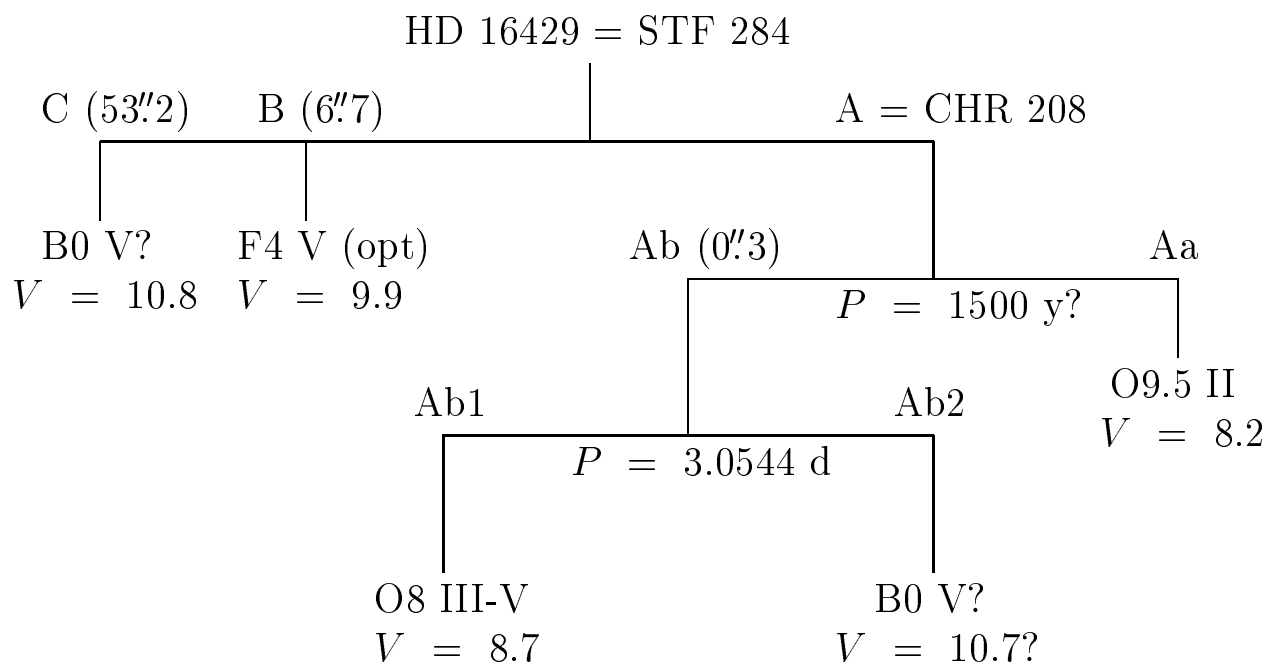


Fig. 1.—

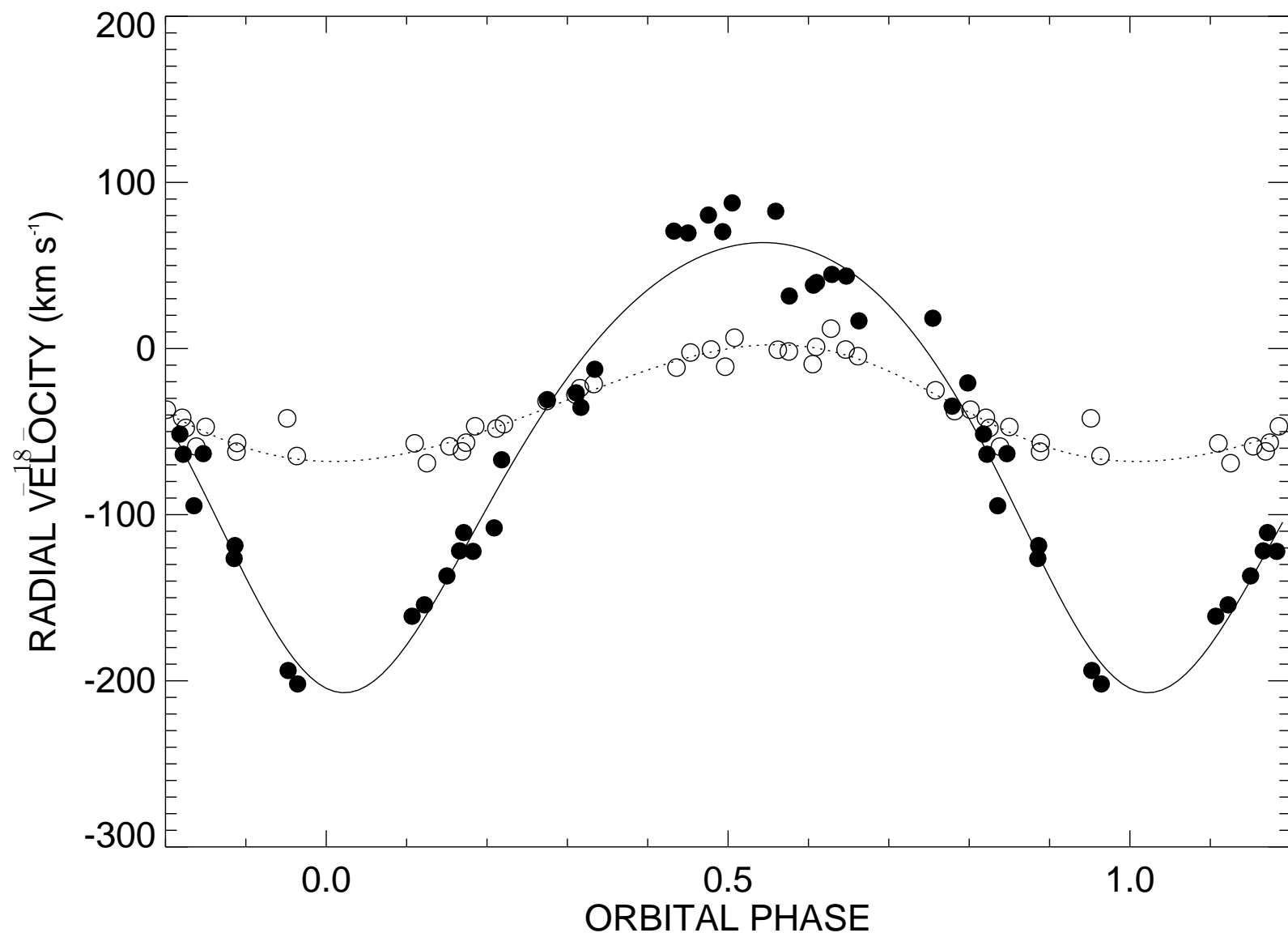


Fig. 2.—

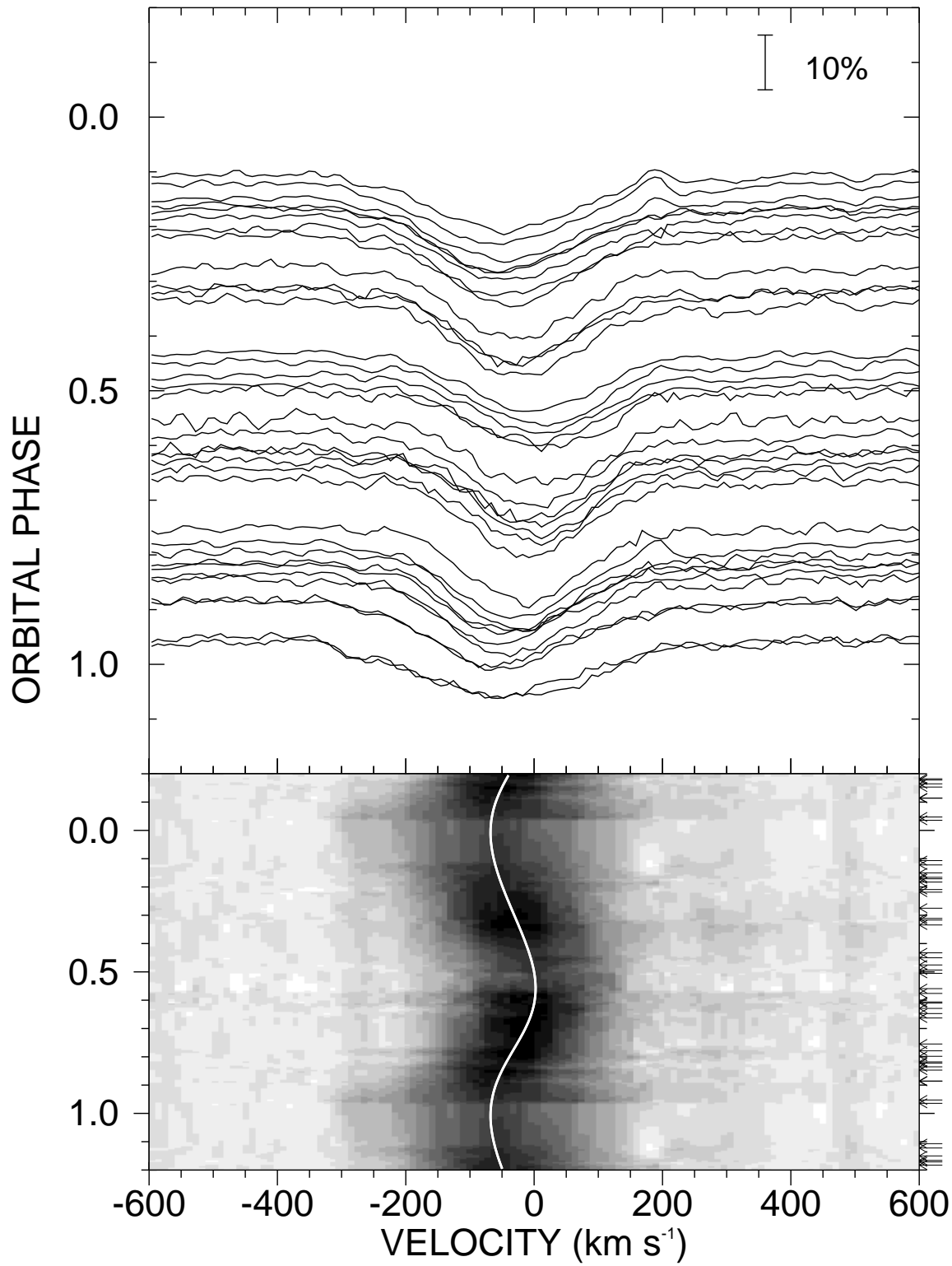


Fig. 3.—

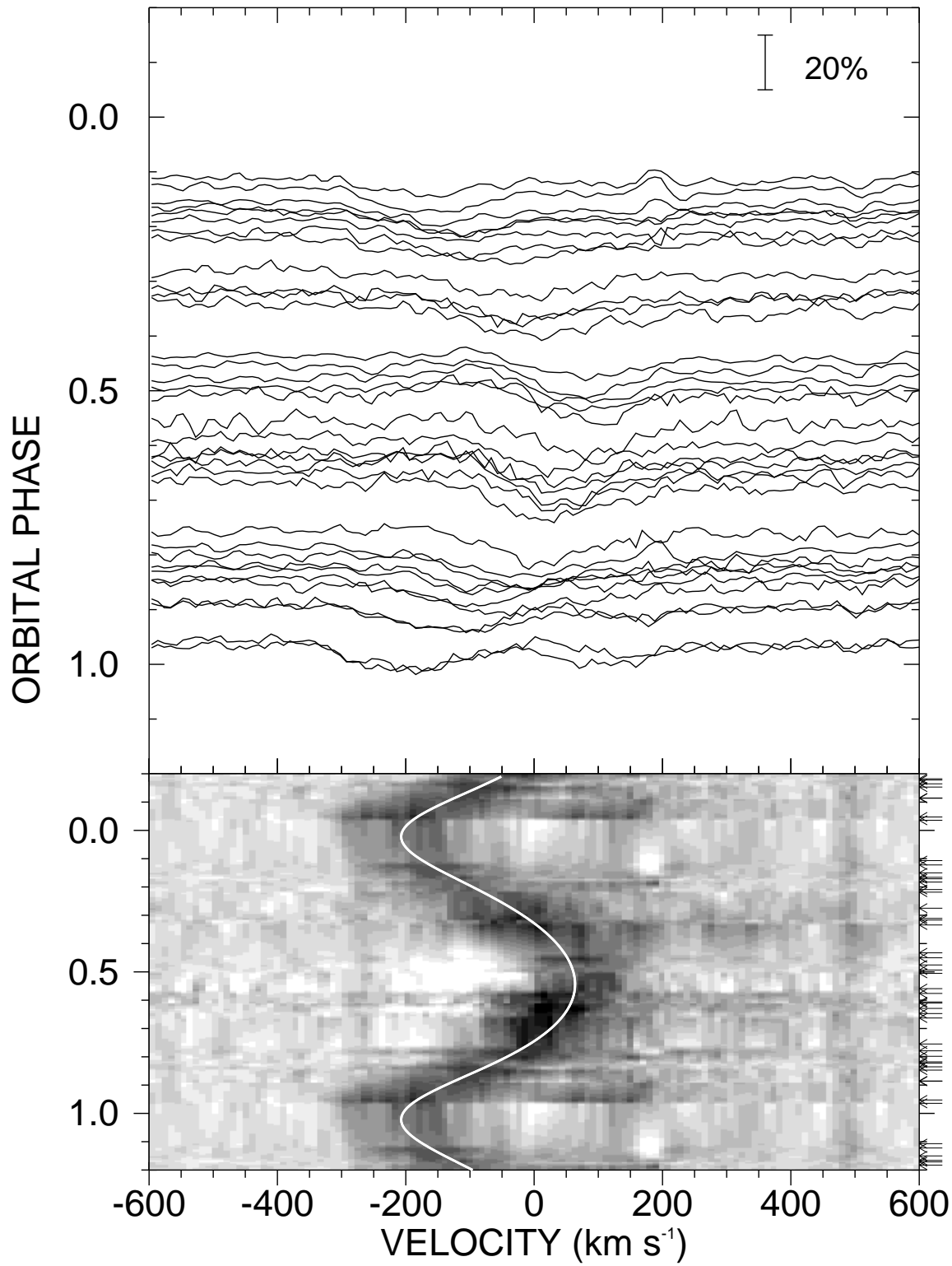


Fig. 4.—

